Mon. Not. R. Astron. Soc. **262,** 603–618 (1993)

Anisotropic induced Compton scattering – constraints on models of active galactic nuclei

P. Coppi,[1,2] R. D. Blandford[2] and M. J. Rees[3]

[1] *Department of Astronomy and Astrophysics, University of Chicago, 5640 South Ellis Ave., Chicago, Illinois 60637, USA*
[2] *Theoretical Astrophysics, California Institute of Technology, Pasadena, CA 91125, USA*
[3] *Institute of Astronomy, Madingley Road, Cambridge CB3 0HA*

Accepted 1992 November 5. Received 1992 November 4; in original form 1992 September 24

ABSTRACT

Induced Compton scattering can cause strong spectral distortion when the Thomson scattering optical depth τ_T exceeds 5×10^9 K/T, where T is the brightness temperature. Observations of intraday variability in several compact radio sources and direct brightness temperature measurements of $\sim 1\text{–}4\times10^{12}$ K from orbiting VLBI prompt a re-examination of this process. We seek observable signatures of induced scattering, using a model for non-linear radiative transfer on a lattice. Induced Compton scattering can significantly increase the brightness temperature at low frequencies and may lead to the formation of steep gradients in the spectrum, and angular discontinuities in the observed intensity. An ultracompact high-brightness core surrounded by a tenuous electron-scattering shell should thus show a faint halo whose spectrum peaks at a lower frequency than the core. Thicker shells can be strongly limb-brightened; frequency-dependent superluminal expansion is also possible. The strongest signatures of induced Compton scattering are strong spectral variation in the source structure and large, frequency-dependent, linear polarization. Under some conditions, stimulated Raman scattering off collective plasma waves, which has similar observational characteristics, may dominate over induced Compton scattering off individual electrons and screened ions. As yet, there is no compelling evidence that induced Compton scattering has been observed in compact radio sources. This implies a (model-dependent) upper limit on the Thomson optical depth of plasma in the vicinity of the source. Future VLBI observations, with greater dynamic range, may provide valuable tracers of dense ionized gas in active galactic nuclei. Infrared observations of blazars should be scrutinized for evidence of induced scattering.

Key words: radiation mechanisms: miscellaneous – galaxies: active – galaxies: nuclei.

1 INTRODUCTION

The discovery of rapid variability in compact extragalactic radio sources inspired several theoretical studies of induced Compton scattering (e.g. Weymann 1965; Goldreich, McCray & Rees 1968; Sunyaev 1970; Melrose 1971; Levich 1972; Zel'dovich & Sunyaev 1972). In this process, low-frequency photons scatter off free electrons at a rate enhanced over the spontaneous rate by the photon occupation number n of the final state. To lowest order, forward and reverse scatterings cancel to give no observable effect. However, when the Compton shift in the frequency ν associated with the electron recoil $\Delta\nu\sim h\nu^2/m_ec^2$ is taken into account, it is found that there is a residual, non-linear contribution to the scattering rate $\sim n\Delta\nu/\nu\sim kT/m_ec^2$ times the spontaneous scattering rate, where $T(\nu)=nh\nu/k$ is the radiation brightness temperature. Induced Compton scattering will therefore cause significant distortion of the emitted spectrum when $T\gtrsim m_ec^2/k\tau\sim(5\times10^9\ \mathrm{K})/\tau$, where τ is the Thomson optical depth of the source. The process can have important consequences in sources with high brightness temperatures, even when the thermal plasma in their environment is 'Thomson-thin'.

Three recent developments in the study of active galactic nuclei (AGN) motivate a re-examination of this mechanism. First, successful trials of orbiting VLBI using the *TDRSS*

satellite (Levy et al. 1989) have shown that several extragalactic compact radio sources contain structure with brightness temperature $T(2.3\ \mathrm{GHz})$ in the range $1\text{–}4\times10^{12}$ K, significantly larger than had previously been measured using earth-bound VLBI (Linfield et al. 1989). Anticipated improvements in the resolution and dynamic range of VLBI maps are expected to be produced by the VLBA (e.g. Romney 1988), *RADIOASTRON* (Kardashev & Slysh 1988) and *VSOP* (Hirabayashi 1991).

The second development is the discovery of 'flicker' (Heeschen 1984) and 'intraday variability' (Quirrenbach et al. 1989) in a variety of compact radio sources. It appears that this variability is present at the 1–2 per cent level in virtually all such sources and at the $\gtrsim 20$ per cent level in roughly a quarter of them (Witzel 1992). The most dramatic example is furnished by the source 0917+624 (Qian et al. 1991), where a formal 'variability brightness temperature' of 2×10^{18} K is measured, some six orders of magnitude above the inverse Compton limit. On the basis of observations of high-brightness, coherent emission in the Sun, Jupiter and radio pulsars, it does not seem unreasonable that coherent emission arises close to a black hole. However, because of effects like induced Compton scattering, it is far more difficult to explain how any such radiation can propagate unchanged through the surrounding medium.

In the third observational development, it has been shown that the far-infrared spectrum in many radio-quiet quasars and Seyfert galaxies turns over sharply at frequencies $\sim10^{12}$ Hz (e.g. Engargiola et al. 1988). Although this turnover is readily interpreted in terms of dust emission (e.g. Sanders et al. 1989), it has also been suggested that it could be due to cyclotron or synchrotron self-absorption (e.g. de Kool & Begelman 1989). Under the conditions suspected to prevail in a galactic nucleus, an infrared synchrotron source that is sufficiently compact to be self-absorbed will probably also be subject to induced Compton scattering. These considerations are also of relevance to blazars, where there is better evidence for a compact non-thermal source.

Motivated by these considerations, we reconsider the signatures of induced Compton scattering within compact extragalactic radio sources. [Induced scattering may also be relevant in pulsar magnetospheres (e.g. Blandford & Scharlemann 1976; Wilson & Rees 1978), masers (e.g. Zel'dovich, Levich & Sunyaev 1972; Garay, Moran & Haschik 1989) and flare stars (Bastian et al. 1990), but we shall not consider these applications in this paper.] As induced Compton scattering is strongly non-linear, most previous analyses (excepting Wilson 1982) have made the simplifying assumption that the radiation field is isotropic and the source homogeneous. However, the scattering medium in an AGN is likely to be more complex, and both assumptions will be poor. Furthermore, the very fact that we can now *resolve* variable synchrotron sources with brightness temperatures $T\gg m_e c^2/k$ invites an extension of these calculations to encompass anisotropic and inhomogeneous source geometry.

In Section 2, we discuss anisotropic induced Compton scattering and explain how an intense beam of radiation may be altered in passing through a slab of plasma that is optically thin to spontaneous Thomson scattering. In Section 3, we describe a numerical approach to induced Compton scattering which involves solving the equations of non-linear transfer on a lattice; we present the results of calculations for some simple geometrical configurations (spheres, discs, cylindrical 'jets', etc.). Some possible applications of these results to the interpretation of actual data on compact radio sources are outlined in Section 4. In Section 5, we briefly consider the far-infrared spectra of AGN. Our conclusions are summarized in Section 6.

2 ANISOTROPIC INDUCED COMPTON SCATTERING

The equation describing the propagation of a beam of low-frequency, high-brightness, unpolarized radiation characterized by an occupation number $n(\nu, \mathbf{\Omega}, \boldsymbol{x}, t)$ along direction $\mathbf{\Omega}$ interacting with cold, free electrons of density $N(\boldsymbol{x}, t)$ is

$$\frac{\partial n}{\partial t}+c(\mathbf{\Omega}\cdot\nabla)\,n = -N\sigma_{\mathrm{T}}cn+\frac{3N\sigma_{\mathrm{T}}c}{16\pi}\int \mathrm{d}\Omega'[1+(\mathbf{\Omega}\cdot\mathbf{\Omega}')^2] \times\left[n'+\frac{2nh}{m_e c^2}\frac{\partial(n'\nu^2)}{\partial\nu}(1-\mathbf{\Omega}\cdot\mathbf{\Omega}')\right] \qquad (1)$$

(e.g. Wilson 1982). For the large occupation numbers of interest, n is related to the brightness temperature by $T=nh\nu/k$. Here $n'=n(\nu, \mathbf{\Omega}', \boldsymbol{x}, t)$. Emission and absorption terms can be added to the right-hand side of this equation. Thermal Doppler shifts, Compton recoil in the spontaneous scattering and polarization effects are, however, ignored. We measure the brightness temperature $T(\nu)$ henceforth in units of the electron rest mass $m_e c^2/k=5\times10^9$ K and introduce a quantity $y=T\nu$ with the dimensions of frequency. y is proportional to the number density of photons per unit frequency per steradian. This general equation is amenable to a variety of simplifications.

First, following Sunyaev (1970), let us suppose that the radiation is isotropic and confined within a volume containing a uniform distribution of free electrons. The radiation will be unaffected by spontaneous scattering and so equation (1) simplifies to

$$\frac{\partial y}{\partial\tilde{t}}=2y\frac{\partial y}{\partial\nu}, \qquad (2)$$

where $\tilde{t}=N\sigma_{\mathrm{T}}ct$. Induced scattering conserves photons but causes them to lose energy in such a way that the quantity y propagates along characteristics in the $(\nu, \tilde{t})$ plane with a constant speed given by $\mathrm{d}\nu/\mathrm{d}\tilde{t}=-2y$. This causes the brightness temperature of the radiation to increase at low frequencies and decrease at high frequencies. If $y(\nu)$ has a maximum at some frequency and a point of inflexion at some lower frequency, then the spectrum at low frequency will steepen and may develop 'shocks'. These shocks can be resolved by reinstating electron recoil and thermal motion (Zel'dovich & Sunyaev 1972). However, the complete Bose condensation of photons to zero energy will ultimately be thwarted by low-frequency absorption.

Next, consider the stationary spectrum arising from a steady source of photons in a region of size R and Thomson optical depth $\tau=N\sigma_{\mathrm{T}}R\lesssim1$ (cf. Sunyaev 1970; Wilson 1982).

We approximate the effects of radiative transfer by adding an escape term $-y/\tau$ to the right-hand side of equation (2) while retaining the assumption of isotropy, and add a power-law source term $\propto \nu^{-(1+\alpha)}$, where α is the usual spectral index. The emergent spectrum will be significantly distorted at frequencies where the optical depth to induced scattering $\tau_i = \tau \partial y/\partial \nu \sim T\tau$ exceeds unity. If we balance emission by frequency change, we find that the steady-state spectrum has a spectral index given by $\max(\alpha/2-1, -1)$. The emergent spectrum is an unbiased sample of the spectrum inside the source (because the escape probability is independent of frequency), and it will therefore have the same shape as the spectrum in the source.

More complex effects are found when the scattering medium is external to the source (cf. Wilson 1982). Consider a scattering slab that is both geometrically and optically thin to spontaneous scattering, but thick to induced scattering, i.e. $T_p^{-1} \lesssim \tau \lesssim 1$, where $T_p(\nu)$ is the brightness temperature of the incident *primary* radiation. Let us suppose that the incident radiation is collimated within a cone of solid angle $4\pi f$ and that its spectrum, specifically $y_p(\nu)$, has a well-defined maximum y_m, at a frequency ν_m similar to that produced by a self-absorbed synchrotron source. α is now the spectral index above the turnover frequency; typically, $0 \lesssim \alpha \lesssim 1$. The primary radiation will be spontaneously scattered more or less isotropically by the electrons in the atmosphere to produce a *secondary* component with spectrum $y_s(\nu)$. For simplicity we treat the secondary radiation as isotropic, though in practice this turns out to be a poor approximation (see Section 3). A crude approximation to equation (1) for the evolution of the primary beam through the slab is then given by

$$-\frac{y_p}{\tau} = -y_p + 3f^2 y_p \frac{\partial y_p}{\partial \nu} + 2y_p \frac{\partial y_s}{\partial \nu} = 0. \tag{3}$$

Now let us consider the secondary radiation. We ignore spatial gradients and just treat its radiative transfer under the escape probability formalism. The secondary radiation intensity will increase as a result of spontaneous scattering by the primary beam, and its spectrum will distort through scattering induced by both the primary and the secondary radiation. This is roughly described by the model equation

$$\frac{y_s}{\tau} = f y_p + 2y_s \frac{\partial}{\partial \nu}(y_s + f y_p). \tag{4}$$

The first terms on the right-hand side of equations (3) and (4) describe the spontaneous scattering from the primary beam to the secondary beam. One factor of f in the second term on the right-hand side of equation (3), which describes self-induced scattering *within* the primary beam, derives from the recoil factor $(1-\mathbf{\Omega}\cdot\mathbf{\Omega}')$. The other factor accounts for the reduced solid angle. The remaining terms describe induced scattering involving the secondary beam.

At high frequency,

$$\nu \gtrsim \nu_1 \sim \nu_m [2f(1+\alpha)\tau T_m]^{1/(\alpha+2)},$$

where $T_m = y_m/\nu_m$, induced scattering can be ignored and the spontaneously scattered secondary spectrum will be

$$y_s \sim \frac{\nu_1}{2(1+\alpha)} \left(\frac{\nu_1}{\nu}\right)^{(\alpha+1)} \qquad \nu \gtrsim \nu_1. \tag{5}$$

However, for $\nu_m < \nu < \nu_1$, the primary beam will induce a downward drift in frequency of the secondary photons. Using equation (4) to balance spontaneous and induced scattering, we find that

$$y_s \sim \frac{\nu}{2(1+\alpha)}; \qquad \nu_m \lesssim \nu \lesssim \nu_1. \tag{6}$$

In other words, the brightness temperature is close to unity. In practice, what generally happens is that the growing secondary component reacts back on the primary beam, reducing its intensity and stimulating the downward migration in frequency of its photons. If the optical depth is large enough, then this mutual induced scattering will saturate when the total flux density in the secondary component is similar to that in the primary beam, i.e., $y_s \sim f y_p$. Below the peak frequency ν_m, we find that y will be roughly constant.

Initially, the secondary component grows exponentially and so the emergent intensity will be extremely sensitive to the path length through the scattering medium and hence to the shape of the scattering medium. For example, when the primary radiation passes through a thin slab, the strongest secondary radiation intensity is found to lie in the slab (the direction with largest optical depth). Naturally, the secondary radiation is a strongly non-linear amplifier of small changes in the primary spectrum.

A separate possibility is that the primary beam may be degraded by self-induced Compton scattering before it scatters into the secondary beam. According to equation (3), this can occur if the brightness temperature of the primary beam satisfies

$$T \gtrsim (3f^2\tau)^{-1}. \tag{7}$$

Self-induced scattering of the primary beam can be very important at frequencies $\nu \gtrsim \nu_m$, where the secondary radiation field is weak, particularly under conditions of high brightness temperature.

Using these arguments, we see that, when high-brightness radio emission propagates through a plasma with induced optical depth $\tau_i \gtrsim 1$, the beam will undergo strong induced scattering, 'initiated' by the spontaneously scattered radiation, on the rising part of the spectrum. Note that, given a beam of high enough intensity, this will take place even when the Thomson optical depth of the plasma is much less than unity. At frequencies below the peak in the spectrum, the compact source will be surrounded by a fainter halo of similar total flux. At high frequencies, where the spectrum is falling, the primary beam ought to emerge from the plasma relatively unchanged, provided that condition (7) is not satisfied.

If the primary beam varies with time, then we expect that both its attenuation and the strength of the secondary component will respond non-linearly. In particular, if the flux at the peak of the primary spectrum changes, then the secondary component can change quickly and a distant observer tuned to a particular frequency might see superluminal effects. Such effects will be highly frequency-dependent.

Inhomogeneity and anisotropy in the radiation field also change the character of the photon 'shocks'. In the special case of a homogeneous source and an isotropic radiation field, the frequency of the shock at a given time is the same

everywhere. This will not be true generally, however, and there will be spatial gradients in the location of the spectral shock in frequency. These are the same as discontinuities in *real space* in the intensity. In this way the radiation from a fairly slowly varying source can mimic that from a point source that changes discontinuously. A distant observer, able to resolve the source, may detect superluminal expansion of the discontinuity, though the total flux will not change discontinuously.

Our discussion of induced Compton scattering has so far ignored collective effects by treating the scattering electrons as independent. This procedure is clearly suspect when the radio wavelengths become comparable with the plasma Debye length $\sim 7(T/1\ \mathrm{K})^{1/2}(n_e/1\ \mathrm{cm}^{-3})^{-1/2}$ cm. Under these circumstances, there are two important changes. First, individual electrons will scatter less effectively because their electric fields will be screened by other electrons. This effect will, however, be compensated by the clustering of electrons around the less mobile ions. As described in Appendix B of Thompson et al. (1992) (cf. also Galeev & Sunyaev 1973), it turns out, quite remarkably, that, under general conditions, this compensation is exact. In other words, the formulae that we have been using for induced Compton scattering remain valid even when the radio wavelength exceeds the Debye length.

The second modification can, however, make a difference. As has been emphasized by, for example, Tsytovich (1970), Melrose (1986), Krishan (1985, 1988) and Thompson et al. (1992), stimulated Raman scattering can become important under these conditions of high brightness temperature. This is a three-wave process in which photons with frequency ω and wave vector $\boldsymbol{k}$ are transformed into waves with frequency $\omega \pm \omega_P$ and wave vector $\boldsymbol{k} \pm \boldsymbol{k}_L$. This process is accompanied by creation or annihilation of electrostatic wave quanta or plasmons with frequency given to good approximation by the plasma frequency $\omega_P = 5.6 \times 10^4 (n_e/\mathrm{cm}^{-3})^{1/2}$, and wave vector $\boldsymbol{k}_L$. Stimulated (or induced) scattering between photon and plasmon states proceeds at a rate proportional to the occupation numbers of the two states. The density of plasmons will be limited by a combination of Landau damping and ion-electron collisional dissipation. Just as with Compton scattering, backscattering can be preferred. As will be discussed in a forthcoming paper (Blandford, in preparation), it turns out in some circumstances that stimulated Raman scattering can be more important than induced Compton scattering.

3 NUMERICAL SIMULATION OF INDUCED COMPTON SCATTERING

The arguments of the previous section are only intended to indicate what physical effects might be important. Equation (1), describing the evolution of an anisotropic photon distribution under the effects of induced Compton scattering, is difficult to solve because, at a given frequency and point in space, the intensity in a particular direction is coupled to the intensity in all other directions. Depending on the sign of the angular integral in equation (1), the intensity in a direction can either decay or grow exponentially. Initially spherically symmetric or isotropic solutions may therefore be unstable to the growth of small perturbations. In addition, compact radio sources are inherently time-dependent, and induced Compton scattering, if important, may significantly amplify any source variations. These considerations motivated us to simulate induced Compton scattering numerically. As the non-linearity in the induced Compton scattering equation is local in space, our attack on the problem will be made in two stages: we first consider the frequency and angular evolution at a particular point in space (i.e., the spatially homogeneous problem); we then attempt to model the effects of spatial transport.

3.1 Homogeneous, anisotropic scattering

We begin by considering the numerical solution of the homogeneous, isotropic scattering equation (2). This is a useful test case as it has the relatively simple implicit solution

$$y(\nu, \check{t}) = y[\nu + 2\check{t}y(\nu, 0), 0], \tag{8}$$

which can be quickly checked against a numerical solution. For $\mathrm{d}y/d\nu > 0$, the spectrum steepens with time, and a shock forms in frequency space at the point where the implicit solution overturns and becomes multi-valued. This behaviour may be seen in Fig. 1. The initial spectrum used in this and subsequent calculations is of the form

$$y(\nu, 0) \propto \nu^{1.5}[1 - \exp(-\nu^{-3})]. \tag{9}$$

Numerically, the infinite gradients that occur in a shock are avoided by introducing a numerical viscosity which enforces diffusion of particles away from the discontinuity. Because the equation being solved is non-linear, the solution near the shock develops a 'ringing instability'. The speed of the characteristics for equation (2) is $\mathrm{d}\nu/\mathrm{d}t \propto -y$, which causes a rarefaction to appear behind an existing shock. As the spectral slope is positive in one part of the rarefaction, that part steepens, forming another shock, and so on. The smaller the numerical viscosity, the larger the amplitude of the resulting shocks. This numerical ('ringing') shock structure is quite physical. Detailed analyses by Zel'dovich & Sunyaev (1972) and Montes (1977) show that the development of infinite gradients due to induced Compton scattering is physically limited by the thermal motions of the scattering electrons. Much like a numerical viscosity, the scattering kernel has a smoothing length associated with it of $\delta\nu/\nu \sim v_e/c$, where v_e is the electron thermal velocity. The fractional width of a shock that develops is correspondingly of this same order. The resulting shock structure, however, is not like a hydrodynamical discontinuity. Rather it is reminiscent of shock models based upon dissipative solitons (e.g. Sagdeev & Galeev 1969; Tidman & Krall 1971). For much the same reasons which lead to the development of an oscillating shock front structure in these models, an analogous 'quasi-line' structure develops in the photon frequency distribution. The numerical viscosity in the numerical scheme which damps out the ringing behaviour can then be thought of as an effective temperature of the scattering electrons. Numerically, the larger the shock amplitude, the smaller the time-step that must be taken and the longer the program execution time. We have therefore chosen a numerical viscosity small enough to keep the leading edge of the first shock sharp, but large enough to suppress most of the quasi-line structure that follows. We restrict ourselves to noting, as did Zel'dovich & Sunyaev (1972), that this shock structure is yet another signature of induced Compton scattering (i.e. strong fre-

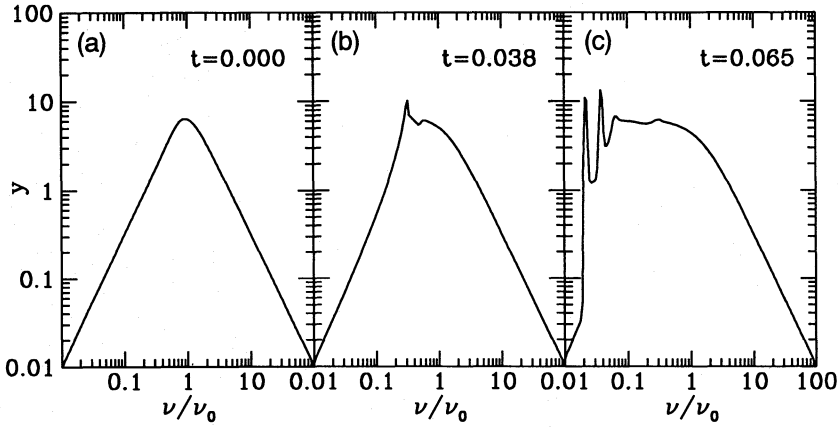

Figure 1. Evolution of a homogeneous, isotropic spectral distribution under the effects of induced Compton scattering. The time t_T is measured in units of the Thomson time $(\sigma_T n_e c)^{-1}$. The initial, $t_T = 0$, spectrum is given by equation (9) with $y_{max} = 10$. Note the steepening of the rising part of the spectrum to form a shock in frequency space. The initial shock is followed by a train of oscillations or shocklets. In practice, the width of these oscillations is controlled by the thermal velocity of the scattering electrons, though here it reflects the artificial viscosity intrinsic to the numerical solver used.

quency dependence). It is not clear, however, that ringing would ever be observable from an actual radio source.

With this caveat, we turn to the problem of solving the frequency evolution equation for an anisotropic distribution. This equation is obtained by dropping the spatial transport term $c(\mathbf{\Omega}\cdot\nabla)n$ from equation (1). We discretize the equation dividing the angular distribution into bins of solid angle. One then obtains a system of coupled differential equations:

$$\frac{\partial y_i(\nu)}{\partial t} = \sum_j c_{ij} y_i \frac{\partial y_j}{\partial \nu}, \tag{10}$$

where the c_{ij} are the angular factors $[1+(\mathbf{\Omega}\cdot\mathbf{\Omega}')^2](1-\mathbf{\Omega}\cdot\mathbf{\Omega}')$ averaged over the solid angle bins i and j. To solve this system, we used a two-tiered, Lax–Wendroff scheme in which values at an intermediate time-step are employed to compute the values at the final time-step. The method seems adequately stable and conserves total photon number well, although it does not explicitly conserve photon number.

The relevant difference equations are

$$y^{n+1/2}_{i,k+1/2} = \frac{1}{2}(y^n_{i,k} + y^n_{i,k+1}) + \frac{\Delta t}{4\Delta \log \nu}\left(\frac{y^n_{i,k}}{\nu_k} + \frac{y^n_{i,k+1}}{\nu_{k+1}}\right)\sum_j c_{ij}(y^n_{j,k+1} - y^n_{j,k}), \tag{11}$$

$$y^{n+1}_{i,k} = y^n_{i,k} + \frac{\Delta t}{2\Delta \log \nu}\left(\frac{y^{n+1/2}_{i,k+1/2}}{\sqrt{\nu_{k+1}\nu_k}} + \frac{y^{n+1/2}_{i,k-1/2}}{\sqrt{\nu_k \nu_{k-1}}}\right) \times \sum_j c_{ij}(y^{n+1/2}_{j,k+1/2} - y^{n+1/2}_{j,k-1/2}). \tag{12}$$

Here the superscript n refers to the time level of the variable (y^{n+1} is y^n evolved by one time-step), the first subscript (i or j) refers to the angular bin, and the second (k) refers to the frequency grid point. Because of the large dynamic range required in frequency, the frequency grid points are spaced logarithmically, with constant separation in $\log(\nu)$ given by $\Delta \log \nu = \log(\nu_k) - \log(\nu_{k-1})$. The boundary conditions imposed for the frequency evolution were no incoming photons at the high-frequency end, i.e. $y^n_{k_{max}+1,j} = 0$, where k_{max} is the index of the highest frequency grid point we evolve, and $y^n_{0,j} = y^n_{1,j}$, the equivalent of a free outflow boundary condition, at low frequency.

To avoid excessive numerical diffusivity, the largest possible time-step consistent with the requirements of numerical stability should be taken. Unfortunately, the usual Courant analysis used to obtain the maximum stable time-step breaks down in our case as the evolution is strongly non-linear. After some experimentation, the time-step constraint was chosen to be

$$\Delta t = \min\{0.9[2\Delta \log \nu/(y^n_{i,k}/\nu_k + y^n_{i,k+1}/\nu_{k+1})], 0.6 y^n_{i,k}/(\mathrm{d}y^n_{i,k}/\mathrm{d}t)\},$$

where i and k run over all possible values and $\mathrm{d}y^n_{i,k}/\mathrm{d}t$ is the estimate of the time derivative used to calculate the intermediate time-step (see equation 11).

3.1.1 *Isotropization of a collimated beam*

In our first example, we consider a collimated beam of radiation with $y(\mu, 0) = y_0$ for $1 \geq \mu \geq 1 - \Delta\mu$ (where $\mu = \mathbf{\Omega}\cdot\mathbf{\Omega}'$) and zero intensity outside the beam. If we only include the induced scattering terms, the beam interacts with itself at a rate reduced by a factor $\sim \Delta\mu^2$ relative to the isotropic case with a similar occupation number. No photons are scattered outside the beam since the occupation number in those directions remains zero (cf. equation 3). However, if we include spontaneous scattering, or a finite background radiation field, induced scattering eventually leads to an exponential growth in the intensity of the radiation field outside the beam (cf. equation 4). The spectral evolution is presented in Fig. 2. The radiation intensity outside the beam, which is initially zero, grows at first through spontaneous Thomson scattering. After a time interval $\propto y_0^{-1}(\Delta\mu)^{-1}$, the rate at which photons are transferred from the beam to a particular

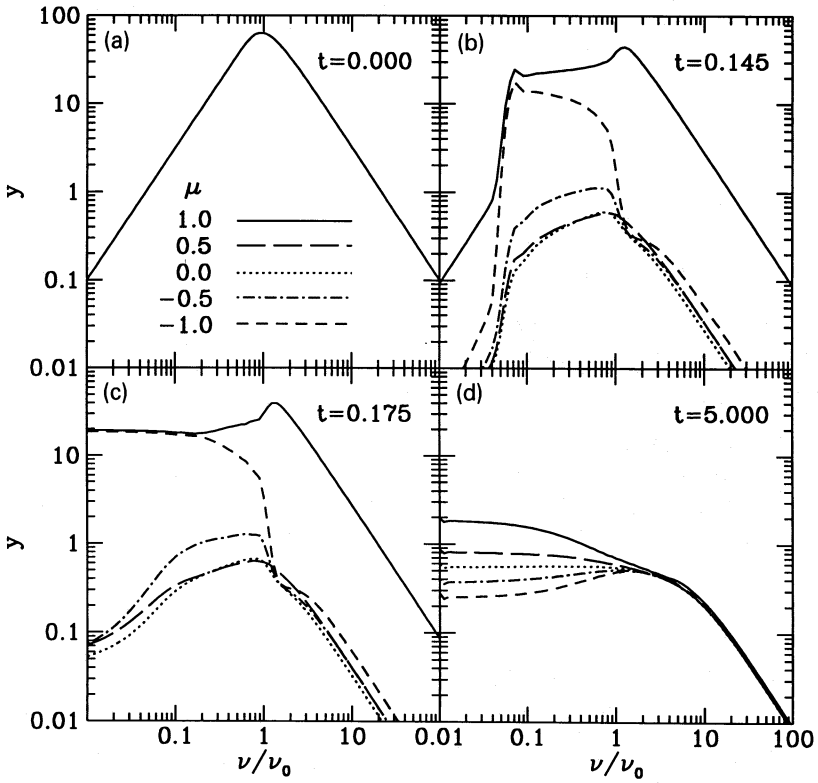

Figure 2. Evolution of an initially beamed spectrum ($\Delta\Omega = \pi/3$) by induced scattering initiated by the spontaneous scattering of photons out of the beam direction. The value of y is plotted at various angles to the beam direction (μ is the cosine of the angle). Note the strong coupling between the forwards and backwards (180 degree) directions which persists for several Thomson times. Note also that the build-up of intensity in the backwards direction, i.e. reflection, occurs on much less than a Thomson time-scale. Asymptotically, y tends to a flat power-law spectrum ($y \sim$ constant) in all directions, although the peak value of y decreases continually with time. When the value of y drops below unity at a given frequency, Thomson scattering dominates and the photon distribution isotropizes at that frequency.

direction by induced scattering equals that due to spontaneous scattering. The intensity in that direction then begins to grow exponentially. The angular factor $(1-\mu)(1+\mu^2)$ in the induced scattering rate (cf. equation 1) ensures that the growth rate is fastest in the direction opposite the beam ($\mu = -1$). Thus, in the simulation, one sees the intensity in the backwards direction rapidly growing to match that in the forwards direction (Fig. 2b). When the intensities in the forwards and backwards directions are approximately equal, they evolve in frequency in a manner similar to that of isotropic radiation, as described above. (The intensity in other directions is much smaller and can be neglected for a time.) The spectrum in these two directions steepens to form a shock (Fig. 2c) which moves downwards in frequency. The presence of a large frequency gradient is then reflected in the spectra at other directions. At a much later time (Fig. 2d), the intensity in other directions builds up and can no longer be neglected, and all directions are coupled. Note that, even after five Thomson times, the angular distribution at low frequencies (where $y > 1$ and induced scattering dominates) has not isotropized. The photon distribution does not completely isotropize until enough photons have migrated to low frequencies to make the peak value of y less than unity.

The salient physical lessons to be drawn from this numerical exercise are, first, that the effects of induced Compton scattering are highly frequency-dependent, in general, becoming more dramatic at lower frequencies. Secondly, the strongest effects are typically seen just behind a frequency shock. The brightness temperature ($\propto y/\nu$) in some directions can be much higher than the peak brightness temperature of the initial photon distribution. However, if the evolution due to induced scattering proceeds too far (e.g. if $y_{\max}\tau_T \gg 1$), the frequency shock will not be observed because the drift to low frequency is too rapid. Even when the scattering medium is Thomson-thin and the radiation is strongly beamed, spontaneous scattering can initiate beam disruption and large reflected flux may be seen at low frequency.

3.1.2 *Instability of isotropic radiation*

As a second numerical example, we consider what happens to a radiation field that has a peaked spectrum and is slightly anisotropic (Gol'din, Sunyaev & Chetverushkin 1975). Again, the evolution of the initial spectrum involves the formation of a frequency shock on the rising side of the spectrum, and the strongest effects are visible just behind the shock. The initial intensity (Fig. 3) is slightly higher in the forwards and backwards ($\mu = 1, -1$) directions. Looking at the induced scattering equation (1), this means that slightly more photons are scattered into the forwards and backwards directions than into the other directions. This in turn means that the frequency shocks in the forwards and backwards directions develop and move slightly faster than those in the

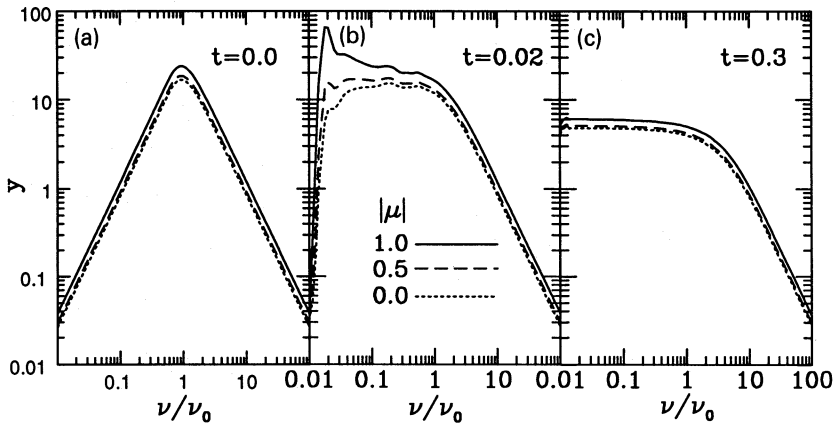

Figure 3. Enhancement of a mild anisotropy by induced Compton scattering. A homogeneous radiation field with a small quadrupolar anisotropy, $y(\mu) \propto 1 + (3\mu^2 - 1)/8$, evolves to amplify the anisotropy. As the frequency shock propagates downwards in frequency, the intensity in the forwards and backwards directions ($\mu = -1, 1$) is amplified at the expense of the intensity in the other directions. At $t_T = 0.023$, the intensity at $\nu = 0.03\ \nu_0$ varies by a factor of three between $\mu = 1$ and $\mu = 0$. Ultimately, the anisotropy at a particular frequency diminishes as the frequency shock propagates to much lower frequencies.

other directions, increasing the scattering rate into these directions at the expense of the spectral evolution in other directions. Behind the shock, the gradient $dy/d\nu$ in the forwards and backwards directions decreases, eventually becoming negative, i.e., at low frequencies the intensity in the other directions is exponentially deamplified and the photon distribution becomes very anisotropic (see Fig. 3b).

The process we have described eventually saturates, and the anisotropy observed at a given frequency eventually decreases (see Fig. 3c). This example illustrates how induced Compton scattering, because of its non-linear nature, can amplify small differences in initial conditions. Again, the magnitude of the effect (in this example, anisotropy) is frequency-dependent and, in general, greatest at the lowest frequencies. As will be seen in the next section, induced Compton scattering can also turn small spatial inhomogeneities in the scattering medium into much stronger inhomogeneities in the emergent radiation field.

3.2 Spatially inhomogeneous, anisotropic scattering

A realistic source model must involve spatial as well as frequency transport of the radiation. We model this using a spatial grid in the form of a face-centred cubic (FCC) lattice (see Fig. 4). At each lattice point we bin the radiation into 12 angular bins directed toward the 12 nearest neighbours. This can be thought of as a 12-stream approximation to radiative transfer. The spectral evolution is computed at each lattice point according to equations (11) and (12) every time-step, and then the radiation is passed between lattice points. This scheme can be parallelized, which leads to a considerable reduction in run time. Not surprisingly, the accuracy of the radiative transfer is greatly improved if the observer direction coincides with one of the 12 directions, as this allows rectilinear propagation at the speed of light. This method has been calibrated by computing the transmission coefficient for an electron-scattering slab. Accuracies of better than one per cent are achievable for optical depths $\tau \lesssim 10$.

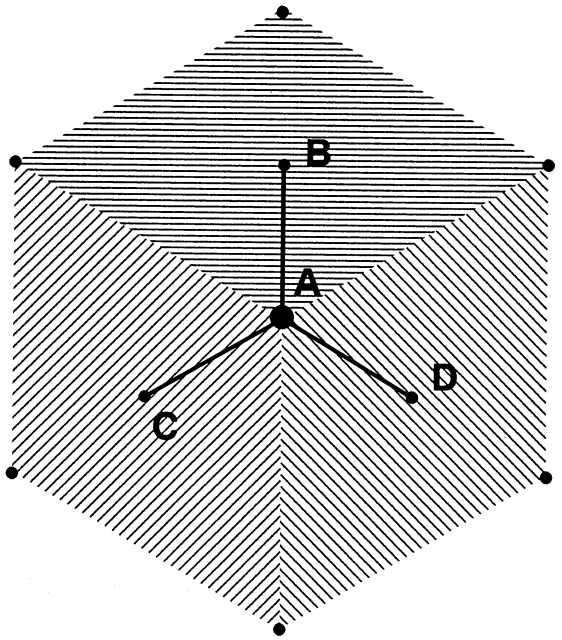

Figure 4. Unit cell of a Face-Centred Cubic (FCC) lattice. The grid point A is shown connected to three of its 12 nearest-neighbour lattice points: B, C, and D.

3.2.1 *Spherical source with scattering shell*

Our first numerical example was also considered by Wilson (1982). A varying spherical source (see Fig. 5a) with uniform emissivity and a self-absorbed synchrotron radiation spectrum is surrounded by a shell of plasma with an optical depth $\tau \sim 0.1$. One octant was modelled by using the FCC lattice and imposing reflecting boundary conditions. The radius, R, of the emitting sphere was roughly four nearest-neighbour spacings. The results are presented in Fig. 6. A cubic spline

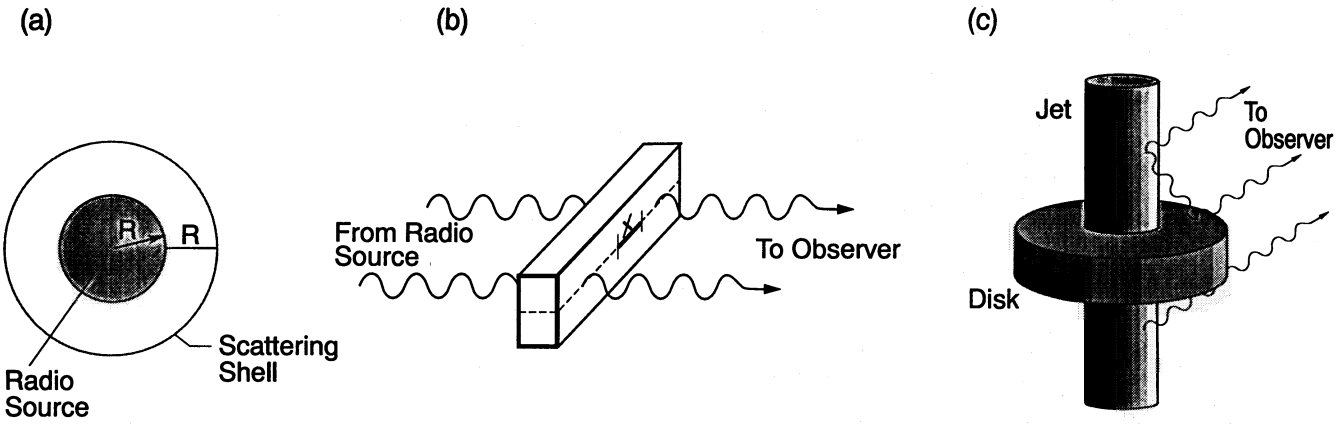

Figure 5. The scattering and source configurations used in the spatially inhomogeneous calculations. See text.

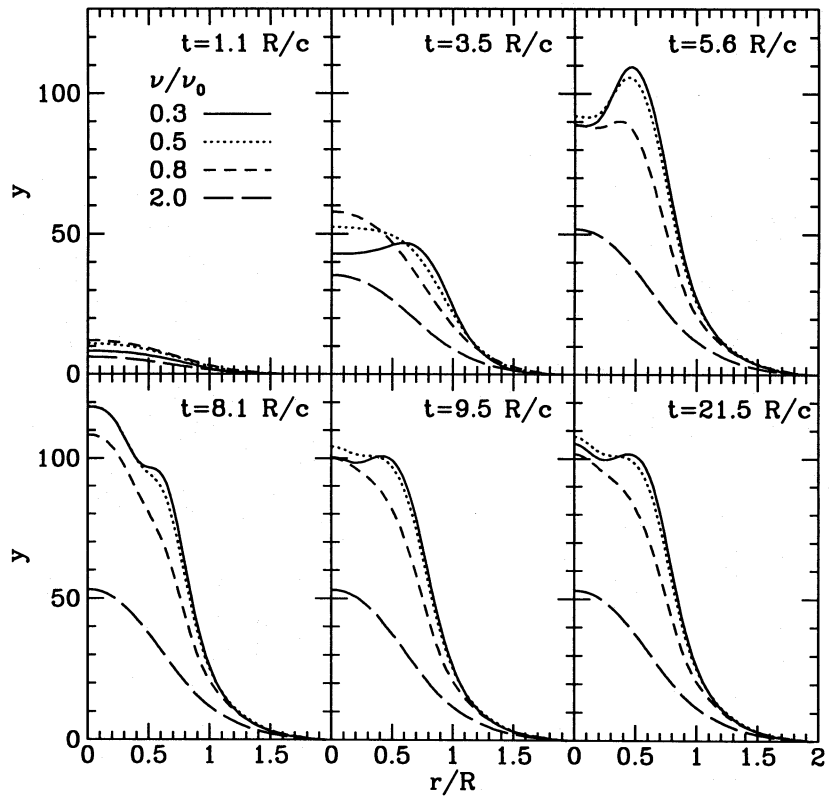

Figure 6. The evolving spatial intensity profile at various frequencies from a spherical source (radius R) of uniform interior emissivity, surrounded by a spherical scattering shell of thickness R and radial Thomson optical depth $\tau_T = 0.1$. The emission is turned on at $t = 0$ and held at a constant value thereafter. The shape of the emission spectrum is the same as in Fig. 1(a) and, in the absence of scattering, $y_{max} \approx 160$ in the outwards direction at the surface of the sphere. Absorption in the source is ignored. The intensity profiles are plotted at frequencies $\nu/\nu_0 = 0.3$, 0.5, 0.8, 2 at $t = 1.1$, 3.5, 5.6, 8.1, 9.5, 21.5 light crossing times (R/c) after the source was turned on. The distance r is the distance from the centre of the projected face of the spherical source. Note the rapid increase of intensity at low frequencies relative to that at high frequencies. Note also the oscillations of the peak brightness across the face of the source and the strong limb brightening (especially at $t = 5.6$).

was used to interpolate the emergent intensity between lattice points. For sources with low brightness temperatures, the sphere appears to be limb-darkened at all frequencies, as the scattering shell is Thomson-thin and we did not include self-absorption effects at low frequencies. The intensity at the surface of the sphere monotonically approaches its steady-state value in a few Thomson times.

The situation changes dramatically when the induced Compton optical depth $\tau_i \gtrsim 1$. Induced scattering becomes important and begins pumping photons to lower energies. The time behaviour in response to the source being turned on also becomes much more complicated. This may be seen in Figs. 6 and 7. The most striking effect seen in this simulation is the temporary limb brightening of the sphere at low

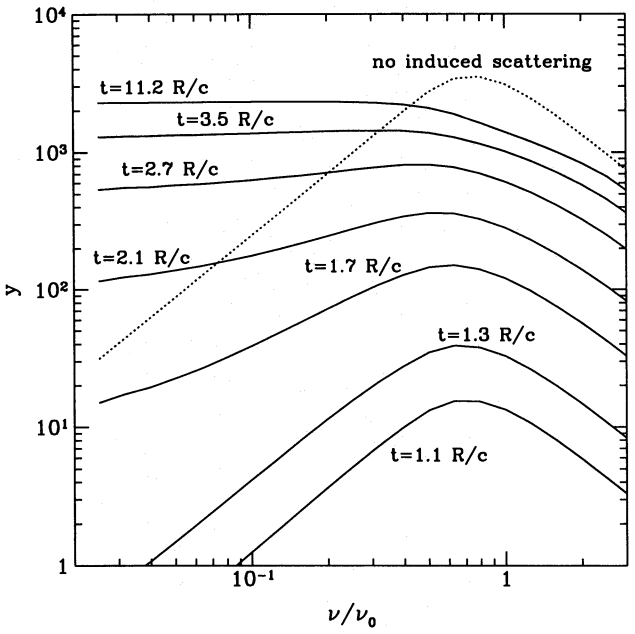

Figure 7. The emergent spectrum integrated over the face of the scattering sphere of Fig. 5(a). The spectrum is shown at $t = 1.1$, 1.3, 1.7, 2.1, 2.7, 3.5, 11.2 light crossing times (R/c) after the source was turned. Note the flattening of the spectrum at late times and low frequencies. Because $y_{\max}\tau_T \gg 1$, a significant number ($\sim 1/4$) of the emitted photons are shifted to frequencies $< 0.01\nu_0$ by induced Compton scattering. The emergent spectrum is quite different from that obtained when induced scattering is turned off (dotted line). Note also that at late times ($t \gtrsim 5.6$) the total spectrum is relatively constant despite the oscillatory limb brightening.

frequencies. The optical depth traversed by a photon reaching the observer is geometrically greatest for photons emitted from the edge of the sphere. Hence the formation and propagation of the frequency shocks takes place first among photons travelling to the observer from the edge of the sphere; so at low frequencies the sphere appears brighter at the edge. As the source intensity builds up, however, more escaping photons have their wave vectors reversed because of the tight coupling between forwards and backwards directions. In a sense, when $\tau_i > 1$, photon escape is impeded. In the spherical problem, the intensity at the limb eventually diminishes and that at the centre of the disc becomes dominant. The result is a damped oscillatory behaviour, with the sphere becoming alternately limb-darkened and limb-brightened with a period related to the light crossing time, R/c.

Another observable property is the integrated spectral variation (Fig. 7). The spectral index varies between zero and 1.5. (The limb-centre oscillations do not appear to affect the averaged spectrum significantly.) As noted by Wilson (1982), even if the source is steady but induced scattering is important, one might also expect to see anomalous spectral indices (inconsistent with the usual synchrotron emission models). Note also that the maximum value of y, and hence the brightness temperature that would be observed (Fig. 7), is significantly reduced by induced scattering. In the case shown, roughly a quarter of the injected photons have condensed to low frequency. This example tells us that a source observed through an atmosphere optically thick to induced scattering may have its peak brightness temperature significantly reduced and its overall size increased.

3.2.2 *Slab with density gradient*

Our second example comprises a collimated radio beam incident normally on a scattering slab (Fig. 5b). The electron density in the slab varies linearly with distance from its centre; this simple model allows us to investigate how inhomogeneities in the optical depth may be amplified by induced scattering. At high frequencies, where the induced scattering is unimportant, the emergent intensity is lowest at the centre where the Thomson optical depth is largest. At frequencies below the incident peak frequency, however, the effect is reversed and the central intensity can be enhanced greatly. Note, though, that there is a threshold effect. At any given point on the slab face, the emergent spectrum looks similar to that exhibited by homogeneous scattering, i.e., it shows a frequency shock. The position of the frequency shock depends on the induced optical depth traversed by the beam in reaching that point on the slab. The higher the optical depth, the lower the shock frequency. If the parameters are such that the frequency being observed falls just below the frequency shock at the edge of the slab and just above it at the centre, a large gradient in intensity will be observed. Induced scattering appears to act as a strongly non-linear amplifier of column density variation, and frquency shocks can be converted into spatial shocks. This amplifier saturates when the optical depth $\tau_i \gg 1$ (see Fig. 8).

This 'threshold effect' (where the intensity at a given frequency jumps rapidly as an intensity shock moves across the slab) can give rise to a type of superluminal motion (see Fig. 9). The delay time between the sharp rise of the intensity at the centre and at the edge can in principle be made arbitrarily small by reducing the density gradient across the slab. In Fig. 9, note also that the relative intensity between the centre and edge oscillates much as it did in the case of the spherical source, and that the distribution at late times is broader than at earlier times.

3.2.3 *Polarization*

In ordinary (spontaneous) Compton scattering, the rate at which radiation is scattered from one direction to another depends on the polarization of the radiation. For a favourable scattering geometry and set of viewing angles, spontaneous Compton scattering can thus generate large degrees of linear polarization. We might expect the non-linearity associated with induced scattering to enhance this effect. In particular, the maximum degree of observed polarization might exceed that obtainable from spontaneous scattering alone, and significant polarization may be generated even if $\tau_T \ll 1$ and one expected Thomson scattering to be unimportant. By analogy with the other effects of induced Compton scattering, one would also expect the degree of polarization produced to vary strongly with frequency, increasing towards lower frequency. Significant linear polarization with a strong frequency-dependence could thus be an important observational signature of induced Compton scattering. The effects of polarization also merit careful consideration because they may lead to results *qualitatively* different from those obtained in an unpolarized calculation. (The scattering

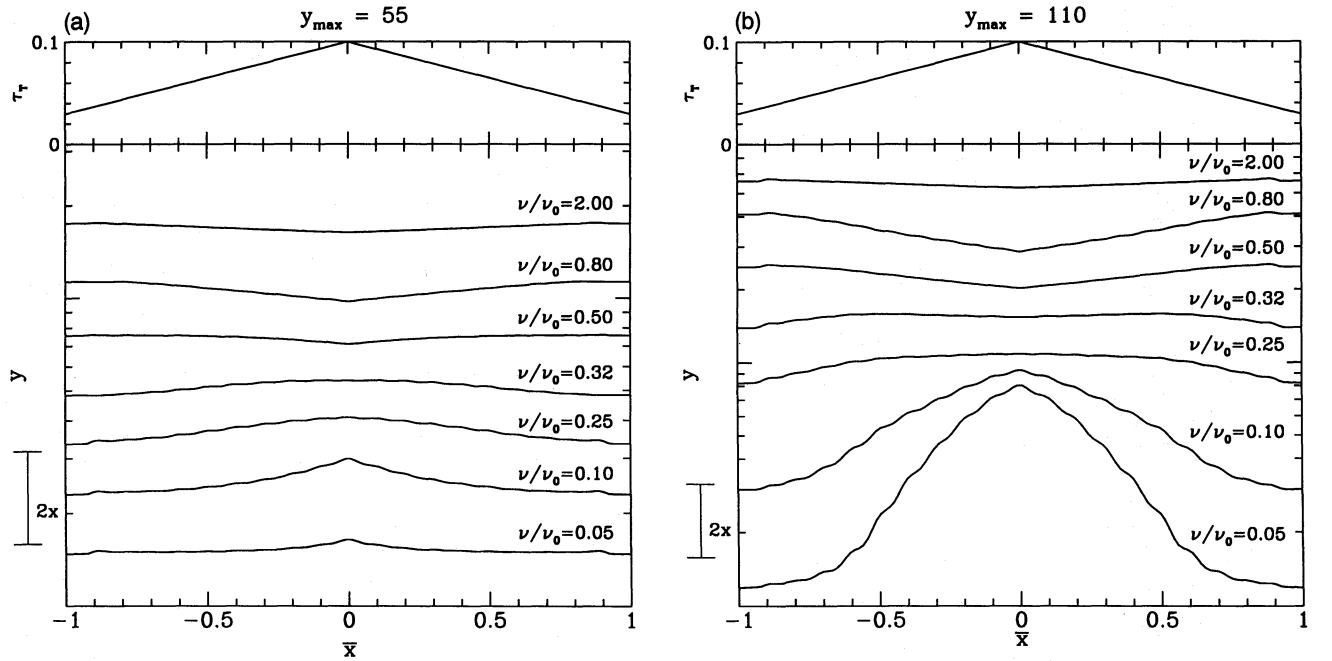

Figure 8. The emergent intensity from a Thomson-thin scattering box of dimensions $5 \times 10 \times 28$ illuminated by plane waves propagating parallel to the shortest edge. The electron density is constant in the direction along the shortest edge of the box, but falls off linearly with distance x (see Fig. 5b) from the centre of the box face. The maximum Thomson optical depth along the shortest dimension of the box is $\tau_T = 0.1$. The emergent intensity along the midplane of the box face and the Thomson depth τ_T are plotted for various frequencies as functions of $\bar{x} = x/X_{slab}$. (X_{slab} is the distance along the midplane from the centre to the edge of the box face.) The shape of the incident radiation spectrum is the same as in Fig. 1a, with $y_{max} = 55$ (panel a) and $y_{max} = 110$ (panel b). The relative intensities of the various frequencies have been rescaled for clarity and to emphasize the contrast between the centre and edge intensities. The scale for y is logarithmic, and a factor of 2 change in intensity corresponds to the height of the bar labelled '2 ×' in the graph. Note that, when induced Compton scattering is important (e.g. the $y_{max} = 110$ case), a moderate gradient in optical depth across the box face leads to an intensity pattern on the box face that looks very different at different frequencies. The intensity at frequencies near the peak of the incident spectrum is deamplified by the migration of photons to lower frequencies, while at low frequencies it may be strongly (non-linearly) amplified.

rates between directions are different from those in the unpolarized case, and this difference can be non-linearly amplified.) The polarization of the incident radiation, for example, might be as important as its degree of anisotropy.

To investigate these possibilities, we repeated the slab and spherical source calculations discussed above, this time keeping track of the polarization. The formal treatment of induced scattering of polarized radiation is quite subtle (Wilson 1982; Coppi, in preparation). It appears, however, that the polarized transfer equation (equation 14) of Wilson (1982), a generalization of equation (1), is sufficient for the incoherent radiation fields likely to be encountered in most astrophysical contexts. We have implemented this equation on our lattice. The preliminary conclusions of our investigation indicate that the total observed intensity does *not* appear to differ qualitatively from that obtained in the unpolarized calculation, at least when the incident radiation is unpolarized. For example, the emergent intensity in the spherical source calculation still showed a strong limb brightening at low frequencies. The intensities measured along particular polarization directions may, however, differ significantly, i.e. induced scattering can indeed produce strong linear polarization. We exhibit this in Fig. 10, where up to ~25 per cent linear polarization was obtained at low frequencies along the limb of the spherical source. The degree of polarization clearly increases with path length through the scattering region and decreases with frequency as expected. It was found that it can exceed that produced by spontaneous scattering alone.

3.2.4 *Jet–disc model*

Finally, we consider a model with no obvious symmetries and an inhomogeneous radiation field. In this example, we have a long, thin source of uniform emissivity, emitting above and below a scattering disc of moderate Thomson optical depth (see Figs 5c and 11). (This case resembles a non-relativistic jet along the rotation axis of an accretion disc.) The system is viewed from an angle such that the receding jet is obscured by the disc. If induced Compton scattering were not important, the bottom jet would appear significantly fainter than the approaching jet because of the obscuring disc. This is indeed the case at high frequencies, whereas at low frequency, where the source brightness temperature is $T \gg 1$, induced scattering becomes important and the image of the *receding* jet can become the more prominent. Again, we see a striking example of frequency-dependent source structure as a result of induced Compton scattering. In Fig. 11, we also find that the reflection of the jet off the disc is considerably enhanced by the backscattering resulting from induced scattering. Induced scattering may allow high-brightness central components to illuminate regions of high

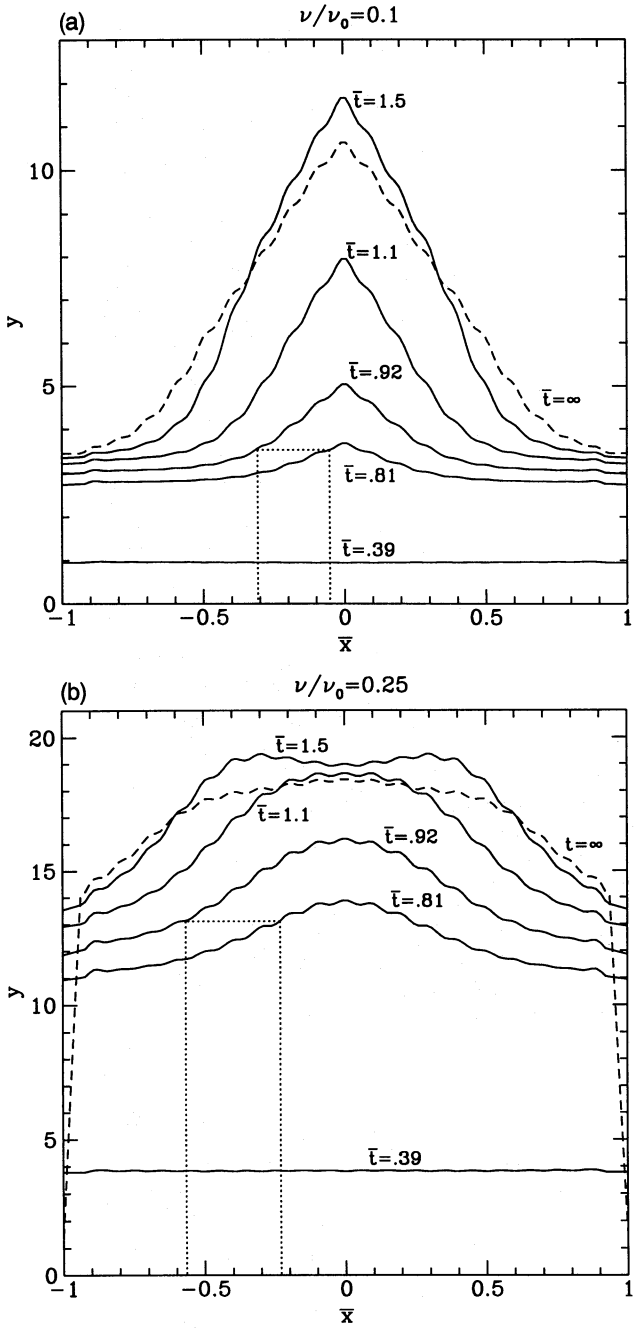

Figure 9. The time evolution of the intensity across the box face (see Figs. 5 and 8) at frequencies $\nu = 0.1\nu_0$ (a) and $\nu = 0.25\nu_0$ (b) in response to an incident intensity that increases linearly from $y_{max} = 0$ at $\bar{t} = 0$ to $y_{max} = 110$ at $\bar{t} = 0.4$ and remains constant thereafter. At all times, the incident spectrum has the form shown in Fig. 1(a). Time is measured in units of $\bar{t} = ct/X_{slab}$, and distance from the centre of the box face is measured in units of $\bar{X} = x/X_{slab}$ (as in Fig. 8). Note the strong non-linear growth of intensity at the centre of the box face after a time $\bar{t} \sim 0.7$ corresponding to the time required for the first photons to reach the front face of the box, be backscattered, and return to the back face of the box. Note that, as in the case of the spherical source (Fig. 6), the relative intensity between the centre and edge of the box face oscillates before settling down to a steady value. At early times, an observer would see a wave of intensity expanding outwards from the centre of the box face. If one defines the edge of the wave to be at some intensity threshold, the wave can appear to expand superluminally ('$c' = \Delta\bar{x}/\Delta\bar{t} \sim 2$–3 in a and b). Note, however, that the source structure and expansion speed are strongly frequency-dependent.

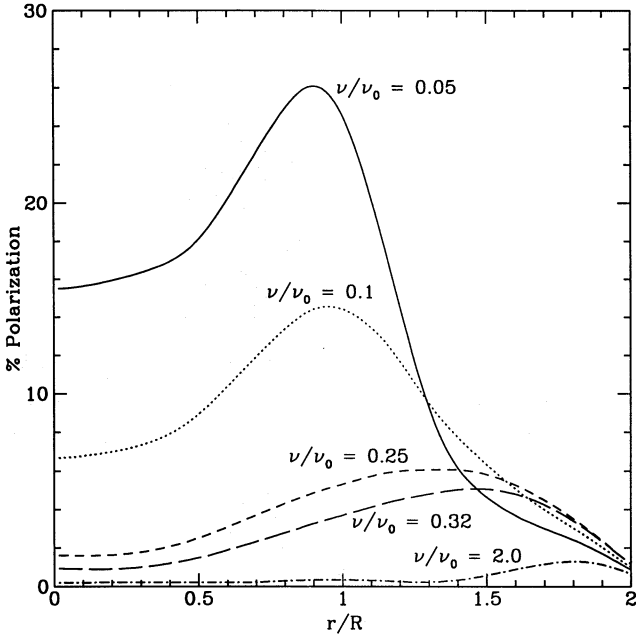

Figure 10. Percentage polarization of the emergent radiation at five different frequencies as a function of distance from the centre of the face of a spherical source surrounded by a scattering shell. The time is $3R/c$ after the source was turned on. The source geometry and the radial Thomson depth of the shell are the same as described in the caption to Fig. 6. The source emissivity is isotropic, unpolarized, and uniform throughout the source region. The shape of the emissivity spectrum is the same as in Fig. 1(a), and $y_{max} \approx 30$ in the outwards direction at the surface of the sphere.

plasma density and these regions may be distinguishable from the source by strong polarization and anomalous spectra.

4 STRUCTURE AND VARIABILITY OF COMPACT RADIO SOURCES

The compact and variable radio components probed by VLBI lie in the central regions of active galaxies. There is, in many cases, direct observational evidence from optical emission lines that these same regions contain photoionized gas. Moreover, there are, quite independently of the optical evidence, strong further indications that the radio source environment must be pervaded by thermal plasma: some inflow of material (either falling in quasi-spherically, or in a disc) is required if accretion provides the primary power source, and the pressure of hot thermal plasma may play a role in confining or collimating the radio jets. It is therefore interesting to explore the consequences of induced scattering by this plasma. Could such effects modify the spectrum and variability of the observed radio emission from compact sources? Could some of the structures revealed by the increasingly refined VLBI 'maps' be due to induced scattering in the environment of the radio source, rather than directly reflecting the shape of the radio-emitting region? And can the radio observations serve as a probe of the spatial distribution of thermal plasma in galactic nuclei, or offer new constraints on its density?

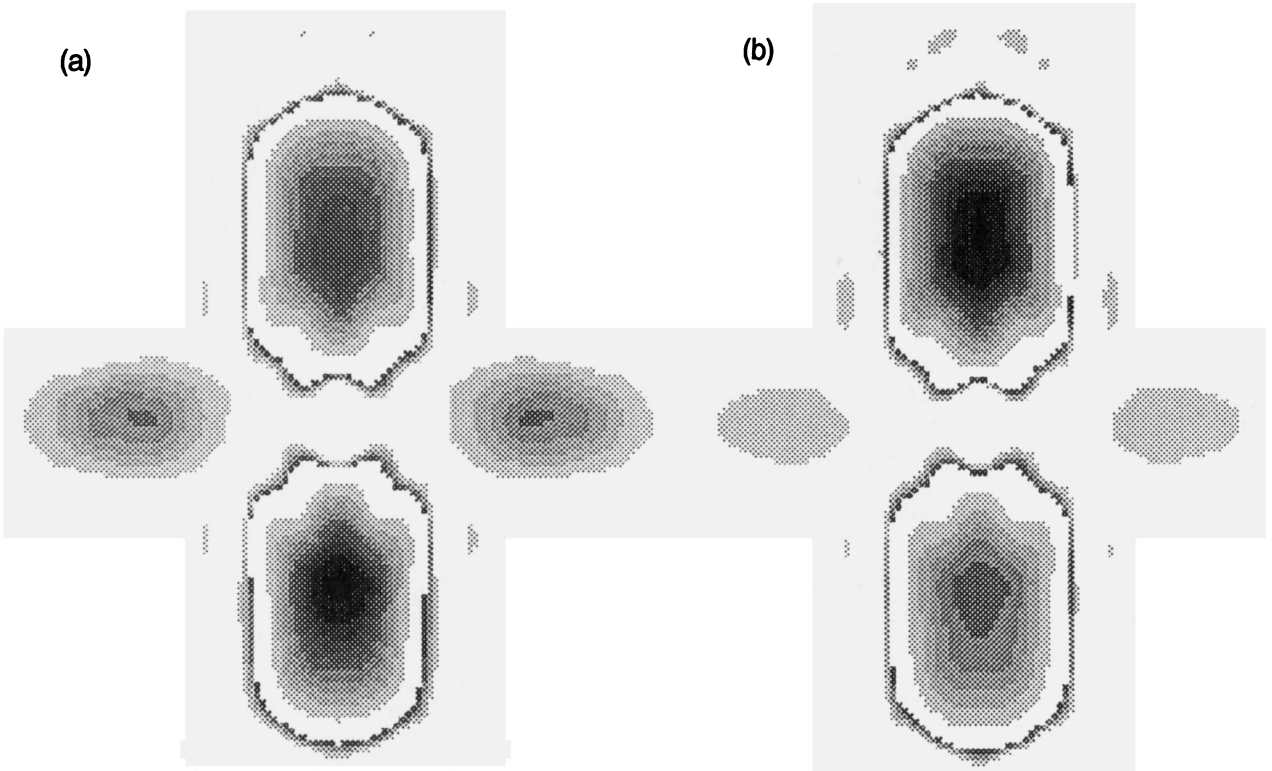

Figure 11. Induced Compton scattering from a jet/disc geometry. A two-sided jet source of uniform (unbeamed) emissivity illuminates a disc of scattering electrons with a Thomson optical depth of 0.4 in the vertical direction (see Fig. 5c). The jet does not penetrate the scattering disc and emerges at a right angle from the disc. The shape of the source emission spectrum is the same as that of Fig. 1(a), and the intensity emerging perpendicular to the sides of the jet has $y_{max} \approx 60$. Inverted grey-scale images are shown of what an observer looking at an inclination angle of 45 degrees and at frequencies $\nu = 0.3\,\nu_0$ (a) and $\nu = 2.0\,\nu_0$ (b) would see. (The brightest areas appear black, the faintest white.) From this vantage point, the bottom jet is partially obscured by the disc. Thus, at frequency $\nu = 2\,\nu_0$ where induced Compton effects are not important, the bottom jet appears darkened relative to the top one because of the considerable Thomson scattering opacity. However, at a lower frequency, $\nu = 0.3\,\nu_0$, induced scattering effects are important and the obscured bottom jet appears *brighter* than the top jet. Note also the faint reflection of the jet off the disc, elongated perpendicular to the jet axis. The ratio of the peak reflected intensity to the peak direct intensity from the jet is enhanced by a factor of ~ 5 at $\nu = 0.3\,\nu_0$ relative to that at $\nu = 2\,\nu_0$. The apparent ring encircling the direct jet emission is an artefact of the algorithm used to interpolate the intensity between grid points.

4.1 VLBI observations

If a radio source of flux density S Jy exhibits strong fringes (with $\gtrsim 50$ per cent visibility) when observed interferometrically with baseline b, the *observed* brightness temperature, T_o, must exceed $\sim 10^{11} S(b/R_\oplus)^2$ K, independent of the observing wavelength, $R_\oplus$ being the Earth's radius. (If the source has a redshift z, the brightness temperature in its own frame is higher by $(1+z)$.) A sample of 24 bright compact radio sources, mostly flat-spectrum quasars, has been observed at a frequency of 2.3 GHz simultaneously by the *TDRSS* satellite and ground-based telscopes (Levy et al. 1989). Fringes were obtained in the majority of cases and 10 sources had inferred source brightness temperatures in the range $T_{12} = (T/10^{12}\,\mathrm{K}) \sim 1$–4 (Linfield et al. 1989). Many of the most powerful compact sources have core-jet structures (Pearson & Readhead 1988). The jets typically have steep spectra ($\alpha \sim 0.5$), and are inhomogeneous and polarized. Bright features tracked with VLBI appear to move superluminally on the sky away from the core. The stationary cores have flat spectra ($\alpha \sim 0$) and are subject to rapid variation.

In a parallel observational development, VLBI has been performed successfully at 3 mm (e.g. Readhead et al. 1983). The peak brightness temperatures inferred from these observations have somewhat smaller lower bounds, typically $\sim 10^{11}$ K.

The standard interpretation of these 'superluminal' sources (e.g. Zensus & Pearson 1987, 1990) is that the jets are collimated outflows of relativistic plasma, moving with Lorentz factors $\gamma \lesssim 10$. The brightest jets, necessarily comprising the sample studied using VLBI, are believed to be directed within $\sim \gamma^{-1}$ to our line of sight with flux densities boosted by a factor $\sim \gamma^{2.5}$. These jets are longer by a factor $\sim \gamma$ than their projected radii $r_\perp$, and larger by a factor $\sim \gamma^2 c$ than the dimensions that would be inferred by straightforward 'light crossing time' arguments from their variability time-scales; hence the superluminal effects. The cores are believed to be the self-absorbed inner parts of the approaching jets. These cores may not be resolved at any frequency, because the observed size of the photosphere varies in a similar manner with frequency as the resolvable linear scale, i.e., $\propto \nu^{-1}$ (Blandford & Königl 1979).

It is generally assumed that the emission mechanism is incoherent synchrotron radiation. In this case, the brightness temperature in the frame of the source is limited to $\sim 10^{12}$ $(\nu/\mathrm{GHz})^{-1/5}$ K; otherwise there would be excessive, and indeed catastrophic, inverse Compton X-ray emission (e.g.

Marscher & Broderick 1985). This argument limits the core brightness temperature in the frame of the AGN at cm wavelengths to $\lesssim 10^{12}\gamma$ K, an inequality which is satisfied by existing observations if indeed $\gamma \sim 10$.

We have argued in Section 3 that the effects of induced Compton scattering should be readily observable if the induced optical depth $\tau_i \gtrsim 1$. If the cores were stationary homogeneous sources, then induced scattering would transform the emergent integrated spectrum into the form $y \sim$ constant, or $S \propto \nu$, at low enough frequency (cf. Fig. 7). (Unfortunately, such a spectrum is not a unique signature of induced Compton scattering, as it can also be produced by an inhomogeneous synchrotron source.) Spatially resolved features like jets should also exhibit strong, frequency-dependent effects like limb brightening (cf. Figs 6 and 8). The observed fluxes of intrinsically variable sources should generally exhibit more pronounced variation at low frequencies than high frequencies (cf. Figs 6 and 8).

The example in Section 3.2.3 shows that polarization can be enhanced by induced Compton scattering, particularly at low frequency and on small linear scales. In realistic radio sources, however, the magnetic field in the scattering medium is probably strong enough for Faraday rotation to be extremely large; the creation of high polarization by induced scattering is therefore unlikely in real sources. If the field is uniform and of strength B G, then the plane of polarization rotates through an angle $\Delta\Phi \sim 4 \times 10^{10} B \nu_9^{-2} \tau_T$ rad, where ν_9 is the frequency in GHz. For the field strengths envisaged in AGN, this is always much larger than unity when the optical depth to induced scattering is large. This would appear to vindicate the use of the unpolarized cross-section, although refraction effects may, in practice, create a 'limiting' polarization.

It is possible that some of the linear features observed with VLBI, for example the complex structure of 3C 84 (Venturi et al. 1992), may not be physical jets analogous to the $\gtrsim$1-kpc jets observed with linked interferometers, but instead radio emission from the core scattered by an elongated cloud or flattened disc of electrons. If this were the case, then we would generally expect that the spectral indices of these features should greatly exceed those of the core components at low frequency.

It is even possible that some of the apparent superluminal expansion observed in compact radio sources is not due to actual relativistic motions, but to time-varying scattering of radio emission from a source which is variable but not itself moving (e.g. Blandford, McKee & Rees 1977; Wilson 1982). We have seen how a burst of radiation normally incident upon a plasma slab is progressively down-scattered in frequency and deflected in direction. Suppose that a compact source is surrounded by a thin spherical shell or circular ring of plasma. Then a distant observer would see an expanding ring in the case of the shell or a pair of separating blobs in the case of a plasma ring. The inferred separation speed can, indeed, be superluminal. (In the case of the ring, the expansion is perpendicular to the source axis.) Again, strong frequency-dependence is anticipated.

There is as yet no clear evidence for any of the above effects, but they have not been actively sought; it may require observations with higher dynamic range (and at two or more different frequencies) to reveal them conclusively. The fact that the effects are not conspicuous in present data is in itself of great interest, because of the constraints thereby placed on thermal plasma in the source environment. Assuming that the effects of induced Compton scattering are not present, we can limit the optical depth in the region surrounding a source. Guided by the spherical model (Figs 6 and 7), we have

$$\tau \lesssim 3 \left(\frac{kT}{m_e c^2} \right)^{-1}. \tag{13}$$

This constrains the electron density around a core of size $\sim r$ from the source to be

$$n_e \lesssim 7000\ T_{12}^{-1}\ r_{pc}^{-1}\ \mathrm{cm}^{-3}. \tag{14}$$

Now let us choose, as an example, a source from the sample of Linfield et al. (1989), namely the $z = 0.352$ quasar $1921-293$ with brightness temperature $T_{12} = 3.8$ and $r_\perp \sim 0.5$ pc. This is not a known superluminal source, but VLBI observations of similar sources suggest $\gamma \sim 6$ (so that the source radius is $r \sim \gamma r_\perp \sim 3$ pc); we then obtain a limit on the free electron density $n_e(3\ \mathrm{pc}) \lesssim 600\ \mathrm{cm}^{-3}$. Of course, a stronger bound can be set at smaller radius, if we ignore the possibility of relativistic motion. As a second example, consider the millimetre-wavelength observations of 3C 84 (Venturi et al. 1992). At 100 GHz, there is an unresolved core of linear size $r_{pc} \sim 0.02$ pc with brightness temperature $T_{12} \gtrsim 0.2$. (There need not be a correction for beaming in this case as the measured source expansion rate is only $\sim 0.2c$; Backer et al. 1987.) Therefore we have the density limit $n_e(0.02\ \mathrm{pc}) \lesssim 10^6\ \mathrm{cm}^{-3}$. Although this is an inferior limit on the optical depth to that derived for $1921-293$, the millimetre-wavelength observations turn out to be more constraining because they are established at a much smaller radius, where the gravitational potential should be dominated by a putative central black hole.

Given an upper bound on the gas density, we can derive an upper bound on the associated gas pressure by assuming that the temperature is less than the escape temperature $T_7 = T/10^7\ \mathrm{K} \sim \max[1, 5 M_{h8} r_{pc}^{-1}]$, where M_{h8} is the mass of the hole in units of $10^8\ \mathrm{M}_\odot$. In both examples, the pressure bounds, $p \lesssim 2 \times 10^{-6}$ dyn cm^{-2} and $p \lesssim 3 \times 10^{-3}$ dyn cm^{-2} respectively, are much smaller than the minimum pressures within the observed radio sources. So it would seem that the thermal gas pressure alone cannot be responsible for jet collimation on these scales (cf. Readhead, Cohen & Blandford 1977). Either the jets are collimated on much smaller scales and essentially propagate ballistically, or magnetic collimation is implicated.

The radio jets observed using VLBI in powerful quasars generally have length scales between those of the broad and the narrow emission-line regions (e.g. Ferland & Rees 1988; Netzer 1991). Pressures can be estimated in both types of line-emitting cloud. It is unclear to what extent there may be a continuous transition between 'broad' and 'narrow' line-emitting regions, but a simple interpolation suggests that the pressure at a typical radius of $r_{pc} \sim 3$ (appropriate to $1921-293$) is $\gtrsim 10^{-4}$ dyn cm^{-2}. If there were a pervasive, Compton-heated, inter-cloud medium (e.g. Krolik, McKee & Tarter 1981), with temperature $\sim 10^7$ K, then its pressure would be limited by the apparent lack of induced Compton scattering to $\lesssim 2 \times 10^{-6}$ dyn cm^{-2}, significantly less than the pressure in the clouds. We therefore conclude that the line-

emitting clouds, like the jets, are not confined by a spherically symmetric distribution of thermal gas. Either the clouds are localized out of the line of sight, or some other confinement mechanism (e.g. magnetic fields) must be invoked.

There is a second, independent argument for there being a significant Thomson depth along the line of sight into an AGN. If the source is powered by steady accretion, there is a minimum quantity of thermal material in each decade of radius. This yields a mean scattering optical depth for all lines of sight down to radius r of

$$\langle\tau\rangle = \varepsilon^{-1}(\dot{M}/\dot{M}_{\rm crit})(v_{\rm freefall}/v_{\rm inflow})(r_{\rm g}/r)^{1/2}, \qquad (15)$$

where $\dot{M}_{\rm crit}$ is the critical accretion rate, and $r_{\rm g} = GM/c^2$. For Eddington-limited, spherical free-fall accretion on to a $\sim 10^8$-$M_\odot$ black hole, with $\varepsilon \simeq 0.1$ (the highest likely value), this estimate gives a minimum mean optical depth at $r \sim 3$ pc of $\langle\tau\rangle \sim 10^{-2}$, corresponding to an electron density $n_{\rm e} \sim 2 \times 10^3$ cm^{-3}. The absence of induced scattering can then be used to argue that gas accretes predominantly through an equatorial plane.

The absence of evidence for induced Compton scattering can already be used to set surprisingly strong upper limits on the gas density along the line of sight in an AGN. What is more exciting, however, is the possibility that future observations made at higher dynamic range with the VLBA and 'World Array' VLBI networks (e.g. Wilkinson 1987) may actually image the densest, accreting, non-emitting plasma (cf. Fig. 11). It may be possible to learn about the basic flow of gas in a galactic nucleus in much the same way that dust reflection nebulae are used at optical wavelengths. This reflected radio emission should also be characterized by strong frequency-dependent reflectivity and high polarization. The recent development of powerful techniques for linear polarization mapping of radio sources using VLBI is particularly important in this regard (Roberts et al. 1990).

The recently identified class of Compact Triple radio sources (Conway et al. 1992) may also turn out to be important. These sources show apparently symmetric radio structure, and it has been argued on morphological grounds that the radio-emitting plasma is not expanding relativistically. They are typically viewed at a large angle to the jet axis. The deprojected distance of the radio components from the nucleus is therefore not much larger than the projected distance (in contrast to the case of 'superluminal' sources), and so the line of sight may well pass through a substantial electron column density.

As discussed briefly in Section 3, reflection through stimulated Raman scattering may be competitive with induced Compton scattering but should cause qualitatively similar effects when present.

4.2 Intraday variability

VLBI observations provided direct measurements of (or upper limits on) radio source brightness temperatures. Variability observations have been used to infer source sizes and hence brightness temperatures indirectly. The most dramatic examples of rapid source variability are the 'intraday variables' reviewed most recently by Witzel (1992). In the source 0917+624 (Qian et al. 1991), a formal 'variability brightness temperature', derived by estimating the source size to be $ct_{\rm var}/(1+z) \sim 10^{15}$ cm, is $\sim 2 \times 10^{18}$ K – seemingly incompatible with synchrotron emission and the inverse Compton limit.

The discussion in Section 2 (equations 5 and 6) showed that induced scattering can yield a low-frequency spectrum $S(\nu) \propto \nu$. It can thereby, in principle, raise the brightness temperature that would be observed below the turnover frequency $\nu_{\rm m}$ by a factor $\sim(\nu_{\rm m}/\nu)$. This effect could not in itself, however, even in an optimal idealized model, make more than a small contribution to reconciling an implied 'variability temperature' of $\gtrsim 10^{18}$ K with the upper limit of $\sim 10^{12}$ K. This is because direct observations, as well as more general energetic constraints, limit $(\nu_{\rm m}/\nu)$ to a value $\lesssim 10$.

Various authors (e.g. Baker et al. 1988) have invoked coherent emission mechanisms to account for these observations. There are several possibilities. Kilogauss magnetic field strengths are expected at distances $\lesssim 10^{15}$ cm from a central black hole, and it is reasonable to suppose that cyclotron maser amplification by mildly relativistic electrons can occur, as in solar and Jovian radio bursts. Alternatively, the characteristic gas density at these distances $n_{\rm e} \gtrsim 10^9$ cm^{-3} (e.g. Rees 1984) has an associated plasma frequency lying in the radio range. High-brightness Langmuir turbulence can be created by mildly relativistic electron beams, and this can be scattered by the same relativistic electrons as electromagnetic waves (Benford 1992). However, the radio brightness temperature would then be so high, and the induced Compton effect potentially so catastrophic, that it would seem barely credible that radio emission originating at $\lesssim 10^{15}$ cm could emerge unchanged through the galactic nucleus. If the radio emission came from a region of radius $\sim 10^{15}$ cm, with brightness temperature T, then the gas density at any larger radius r, along the line of sight, would have to satisfy

$$n_{\rm e}(r) \lesssim 10 \left(\frac{T}{10^{18}\,{\rm K}}\right)^{-1} \left(\frac{r}{10^{15}\,{\rm cm}}\right)^{3} {\rm cm}^{-3} \qquad (16)$$

(cf. equation 7). For the extreme case of 0917+624, this requires an ambient density $n_{\rm e} \lesssim 10$ cm^{-3} at $r \sim 10^{15}$ cm, up to 10 orders of magnitude smaller than the typical plasma density required in the source region to sustain the observed power.

Even if both the accreting gas and the broad-line region are confined to a disc inclined at a large angle to the line of sight which is efficiently evacuated, Thomson scattering may be unavoidable for another reason. In compact sources of hard X-rays and γ-rays, the compactness parameter $\ell = L_\gamma \sigma_{\rm T}/R m_{\rm e} c^3$ is a measure of the probability that two 1-MeV photons will create an electron–positron pair before escaping from the source. Even if there were no other matter present, the resultant pairs would contribute a Thomson optical depth of $\sim 0.3\,\ell^{1/2}$ (for $\ell > 1$) and at least $\sim \ell$ (for $\ell < 1$). So those AGN that are intense compact γ-ray sources are likely, for independent reasons, to have an appreciable induced scattering optical depth.

If these rapidly variable radio sources are not as compact as indicated by naive arguments, then alternative explanations for the variability must be sought. The two most favoured are relativistic expansion with Lorentz factors that may have to be as large as $\gamma \sim 100$, or refractive scintillation in our interstellar medium. The merits and difficulties associ-

ated with both explanations have been reviewed elsewhere (e.g. Witzel 1992).

5 FAR-INFRARED EMISSION FROM RADIO-QUIET QUASARS

The nature of the infrared continuum emission observed from quasars has long been controversial. Competing proposals include non-thermal synchrotron radiation (e.g. Begelman 1989), Comptonized cyclotron radiation (e.g. Takahara, Tsuruta & Ichimaru 1981), re-radiation of UV from a central accretion disc by circumnuclear dust (e.g. Sanders et al. 1989) and inverse Compton radiation (e.g. Band & Grindlay 1986). The majority of quasars are radio-quiet and so their spectra must turn over at far-infrared wavelengths. Sub-mm observations of radio-quiet quasars by, for example, Edelson et al. (1988), Engargiola et al. (1988) and Keene et al. (1989) have shown that the flux must rise very rapidly beween sub-mm and far-infrared wavelengths, with a spectral index that may be as negative as -2.5, the slope of the emission from a homogeneous, optically thick synchrotron source. Most conceivable forms of inhomogeneity will flatten the spectrum (but see de Kool & Begelman 1989), so if this type of spectrum turns out to be typical, then a synchrotron origin for the infrared continuum can probably be ruled out.

A self-absorbed, ~ 100-μm infrared synchrotron source in a bright quasar would have a luminosity $\sim 10^{46}$ erg s^{-1} and a size $R \sim 5 \times 10^{15} (T/10^{12}\,\mathrm{K})^{-1/2}$ cm, where T is the brightness temperature. With a source so compact, the induced Compton optical depth is likely to exceed unity and the emergent spectrum will be altered. If the synchrotron source is embedded in the plasma, however, and is quasi-stationary as the observations suggest, then the low-frequency spectrum would not be as steep as observed (cf. de Kool, Begelman & Sikora 1989). The only way to obtain a spectrum rising steeply with frequency via induced Compton scattering would be to produce a photon shock, but the spectrum shortward of this shock would then be $S \propto \nu$, in contrast to the observed $S \propto \nu^{-1}$. Moreover, the location of the shock in frequency would be sensitive to inhomogeneities in the plasma density. When integrated over the source region, the total flux again would probably not show as steeply rising a spectrum.

Perhaps the best prospect for observing induced Compton effects in AGN lies with the blazars and the compact radio quasars, in which the infrared emission is reportedly variable and polarized. The infrared peak has been hypothesized to be synchrotron emission from the innermost parts of a relativistic jet beamed in our direction. Indeed, in many sources, we may actually be viewing this source through the jet. Alternatively, the non-thermal emission from blazars may originate from an isotropic, self-absorbed synchrotron source. This would be likely to contain electrons and positrons and consequently have an appreciable Thomson depth, as discussed in Section 4. The millimetre-wave spectra are typically flat and could accommodate induced Compton scattering. The maximum brightness temperature in the infrared may then be limited by induced scattering to $\sim 10^{10}$ K, rather than to the higher value of $\sim 10^{12}$ K characteristic of synchrotron self-absorption. It is well worth seeking the characteristic induced Compton flux variation, a flattening of the spectrum towards $S \propto \nu$ (in the wake of the photon shock), following an outburst in one of these sources.

6 DISCUSSION

We have shown that induced Compton scattering leads to new and potentially observable effects in active galactic nuclei in the radio–infrared region of the spectrum. Induced scattering may be recognizable in images, integrated spectra and variability through its frequency variation and polarization. None of these predicted effects has been unambiguously observed. All VLBI data seem so far to be consistent with the simplest type of relativistic jet model, in which the radio core is self-absorbed and the jet is surrounded by extremely tenuous plasma. Lorentz factors as large as $\gamma \sim 100$ may be necessary to account for the most dramatic variability if this is shown to have an intrinsic origin. The effects of induced scattering would have been observed already if the core size were independent of frequency and no larger than the upper bound determined at high frequency. Unless there is some entirely new class of extragalactic source (e.g. a coherent emitter whose surroundings are swept clean by an ultrarelativistic outflowing wind, as in the Crab nebula), we suspect that all radio sources at cosmological distances will be essentially resolved by interferometers that can measure brightness temperatures in excess of $\sim 3 \times 10^{13}$ K. The space interferometry mission *RADIO-ASTRON* (e.g. Kardashev & Slysh 1988), which is planned to operate up to 22 GHz with a maximum baseline of $\sim 12\,R_{\oplus}$, will be especially revealing in this context.

Extragalactic radio sources clearly constitute a heterogeneous class of objects, and there may well be a few examples showing unusual behaviour manifesting the effects of induced scattering. In particular, it may be possible to highlight the gas flow in an AGN using VLBI observations of reflected radio waves. In addition, as we have argued, spectral and variability studies of far-infrared emission from blazars may point to the presence of induced Compton scattering in a minority.

ACKNOWLEDGMENTS

We thank Sterl Phinney, Tony Readhead and George Rybicki for valuable suggestions and critical comments on an earlier draft of this paper. RB thanks the Institute of Astronomy for hospitality during 1987 July–August when this work was begun and the Harvard–Smithsonian Center for Astrophysics for further support. NSF grant AST-89-17765 and NASA grants NAGW-830, NAGW-1284, NAGW-1301, NAGW-1636 and NAGW-2816 are also gratefully acknowledged.

REFERENCES

Backer D. C. et al., 1987, ApJ, 322, 74
Baker D. N., Borovsky J. S., Benford G., Eilek J. A., 1988, ApJ, 326, 110
Band D. L., Grindlay J. E., 1986, ApJ, 308, 576
Bastian T. S., Bookbinder J., Dulk G. A., Davis M., 1990, ApJ, 353, 265
Begelman M. C., 1989, in Osterbrock D. E., Miller J. S., eds, Proc. IAU Symp. 134, Active Galactic Nuclei. Kluwer, Dordrecht, p. 141

Benford G., 1992, ApJ, 391, L59
Blandford R. D., Königl A., 1979, ApJ, 232, 34
Blandford R. D., Scharlemann E. T., 1976, MNRAS, 174, 59
Blandford R. D., McKee C. F., Rees M. J., 1977, Nat, 267, 211
Conway J. E., Pearson T. J., Readhead A. C. S., Unwin S. C., Xu W., Mutel R. L., 1992, ApJ, 396, 62
de Kool M., Begelman M. C., 1989, Nat, 338, 484
de Kool M., Begelman M. C., Sikora M., 1989, ApJ, 337, 66
Edelson R A., Gear W. K. P., Malkan M. A., Robson E. I., 1988, Nat, 336, 749
Engargiola G., Harper D. A., Elvis M., Willner S. P., 1988, ApJ, 332, L19
Ferland G., Rees M. J., 1988, ApJ, 332, 141
Galeev A. A., Sunyaev R. A., 1973, Sov. Phys. JETP, 36, 669
Garay G., Moran J. M., Haschik A. D., 1989, ApJ, 338, 244
Gol'din V. Ya., Sunyaev R. A., Chetverushkin B. N., 1975, Sov. Phys. JETP, 41, 18
Goldreich P., McCray R., Rees M. J., 1968, Nat, 217, 931
Heeschen D. S., 1984, AJ, 89, 1111
Hirabayashi H., ed., 1991, Frontiers of VLBI. Academic Press, Tokyo
Kardashev N. S., Slysh V. I., 1988, in Reid M. J., Moran M. J., eds, Proc. IAU Symp. 129, The Impact of VLBI on Astrophysics and Geophysics. Kluwer, Dordrecht, p. 441
Keene J., Neugebauer G., Carico D., Sanders D., Soifer B. T., 1989, in Osterbrock D. E., Miller J., eds, Proc. IAU Symp. 134, Active Galactic Nuclei. Kluwer, Dordrecht, p. 396
Krishan V., 1985, Ap&SS, 115, 119
Krishan V., 1988, MNRAS, 230, 183
Krolik J. H., McKee C. F., Tarter C. B., 1981, ApJ, 249, 422
Levich E. V., 1972, Sov. Phys. JETP, 34, 59
Levy G. S. et al., 1989, ApJ, 336, 1098
Linfield R. P. et al., 1989, ApJ, 336, 1105
Marscher A. P., Broderick J. J., 1985, ApJ, 290, 735
Melrose D. B., 1971, Ap&SS, 10, 186
Melrose D. B., 1986, Instabilities in Space and Laboratory Plasmas. Cambridge Univ. Press, Cambridge
Montes C., 1977, ApJ, 216, 329
Netzer H., 1991, in Blandford R. D., Netzer H. & Woltjer L., eds, Active Galactic Nuclei. Springer-Verlag, Berlin, p. 57
Pearson T. J., Readhead A. C. S., 1988, ApJ, 328, 114
Qian S. J., Quirrenbach A., Witzel A., Krichbaum T., Hummel C. A., Zensus J. A., 1991, A&A, 241, 15
Quirrenbach A., Witzel A., Qian S. J., Krichbaum T., Hummel C. A., Alberdi A., 1989. A&A, 226, L1
Readhead A. C. S., Cohen M. H., Blandford R. D., 1977, Nat, 272, 131
Readhead A. C. S. et al., 1983, Nat, 303, 504
Rees M. J., 1984, ARA&A, 22, 471
Roberts D. H., Wardle J. F. C., Brown L. F., Gabuzda D. C., Cawthorne T. V., 1990, in Zensus J. A., Pearson T. J., eds, Parsec-scale Radio Jets. Cambridge Univ. Press, Cambridge, p. 110
Romney J. D., 1988, in Reid M. J., Moran M. J., eds, Proc. IAU Symp. 129, The Impact of VLBI on Astrophysics and Geophysics. Kluwer, Dordrecht, p. 441
Sagdeev R. Z., Galeev A. A., 1969, Nonlinear Plasma Theory. W. A. Benjamin, New York
Sanders D. B., Phinney E. S., Neugebauer G., Soifer B. T., Matthews K., Green R. F., 1989, ApJ, 347, 29
Sunyaev R. A., 1970, Astrophys. Lett., 7, 19
Takahara F., Tsuruta S., Ichimaru S., 1981, ApJ, 251, 26
Thompson A. C., Blandford R. D., Evans C. R., Phinney E. S., 1992, ApJ, submitted
Tidman D. A., Krall N. A., 1971, Shock Waves in Collisionless Plasmas. Wiley, New York
Tsytovich V. N., 1970, Nonlinear Effects in Plasmas. Plenum Press, New York
Venturi T., Readhead A. C. S., Marr J. M., Backer D. C., 1992, preprint
Weymann R., 1965, Phys. Fluids, 8, 2112
Wilkinson P. N., 1987, in Zensus J. A., Pearson T. J., eds, Superluminal Radio Sources. Cambridge Univ. Press, Cambridge, p. 211
Wilson D. B., 1982, MNRAS, 200, 881
Wilson D. B., Rees M. J., 1978, MNRAS, 185, 297
Witzel A., 1992, in Wagner S., Duschl W. J., eds, Physics of Active Galactic Nuclei. Springer-Verlag, Heidelberg, p. 484
Zel'dovich Ya. B., Sunyaev R. A., 1972, Sov. Phys. JETP, 35, 81
Zel'dovich Ya. B., Levich E. V., Sunyaev R. A., 1972, Sov. Phys. JETP, 35, 733
Zensus J. A., Pearson T. J., 1987, Superluminal Radio Sources. Cambridge Univ. Press, Cambridge
Zensus J. A., Pearson T. J., 1990, Parsec-scale Radio Jets. Cambridge Univ. Press, Cambridge